Materials and Methods

Reagents. Rhodamine-phalloidin was from Cytoskeleton, Inc. (Denver, CO). 4', 6-diamidino-2-phenylindole (DAPI) was from Invitrogen (Carlsbad, CA). LPA was from Avanti Polar Lipids, Inc. (Alabaster, AL). Restriction enzymes were either purchased from New England Biolabs (Ipswich, MA) or Promega (Madison, WI). All other chemicals were from Sigma-Aldrich (St. Louis, MO) unless otherwise specified.

Tyrosinated α-tubulin rat mAb (YL1/2) was from the European Collection of Animal Cell Cultures (Salisbury, UK). GFP mouse mAb was from Sigma-Aldrich. β-catenin mouse mAb and rabbit polyclonal antibody were from Zymed (San Francisco, CA). Mouse mAb and rabbit polyclonal pericentrin antibody were from Covance (Princeton, NJ). Emerin mouse mAb antibody was from Novacastra Laboratories (Newcastle upon Tyne, UK). Polyclonal rabbit antibodies against SUN1 and SUN2 were provided by S. Shackleton (Leicester University, UK). LBR guinea pig polyclonal antibody was provided by H. Herrmann (German Cancer Research Center, Heidelberg, Germany). Lamin A/C mouse mAb (MANLAC1) was provided by G. Morris (MRIC Biochemistry Group, Wrexham, UK). Lamin B1 mAb was provided by H. Worman (Columbia University, NY). LAP1 rabbit polyclonal antibody was provided by William Dauer (University of Michigan, MI). mDia1 mouse monoclonal antibody was from BD Transduction (Lexington, KY). mCherry-Lifeact plasmid was provided by R. Wedlich-Soldner (Max Planck Institute of Biochemistry, Martinsried, Germany)

Cell culture and monolayer wounding. NIH3T3 fibroblasts were cultured in DMEM with 10% bovine calf serum (Thermo Fischer Scientific, Waltham, MA); serum starved for 2 days, wounded and stimulated with 10 μM LPA as previously described (*1, 2*). NIH3T3 fibroblasts stably expressing GFP-α-tubulin (*1*) were grown in DMEM with 10% bovine calf serum containing 1 mg/mL G418 sulfate (Calbiochem, Darmstadt, Germany) and treated as described above for NIH3T3 fibroblasts.

RT-PCR. Isolation of mRNA from NIH3T3 fibroblasts, mouse brain and testis was with Trizol (Invitrogen) according to the manufacturer's protocol. RT-PCR was performed with SuperScript™ III One-Step RT-PCR System (Invitrogen) using the primers described in Table S1.

DNA constructs. SR-KASH, KASH and KASHΔL were amplified by PCR from human clone nesprin2 clone LIFESEQ526866 (Open Biosystems, Surrey, UK) using primers described in Table S2. PCR products were inserted into pmRFP-C1 vector, a gift from E. Marcantonio (Columbia Univ., NY). RFP-C1 encodes monomeric red fluorescent protein (mRFP1) inserted in place of GFP in pEGFP-C1 (Clontech Laboratories, Inc., Mountain View, CA). SUN2 full length was PCR amplified from mRNA isolated from NIH3T3 fibroblasts, and cloned into pEGFP-C1 using *Sal*I and *Xba*I.

To generate the GFP-mini-nesprin2G construct, DNA sequences corresponding to the N-terminal CH domains (aa 3-483), and the two C-terminal spectrin repeats and KASH domain (aa 6517-6874) of nesprin2G (XM_917083) were amplified by RT-PCR from NIH3T3 fibroblast mRNA and inserted into pmRFP-C1 after digestion with *Sal*I and *Xba*I. To fuse the N-terminal and C-terminal fragments we performed splicing by overlap extension (SOEing) PCR. The resulting fusion was subcloned into pEGFP-C1 to create GFP-mini-nesprin2G. Three silent point mutations were generated in GFP-mini-nesprin2G to make it resistant to siRNA using Quikchange site directed mutagenesis kit according to the constructer protocol (Stratagene, La Jolla, CA). To generate GFP-mini-nesprin2GΔCH, we amplified the region of DNA encoding aa 315-483 from GFP-mini-nesprin2G and subcloned the PCR product into pEGFP-C1 using *Sal*I and *Xba*I. GFP-mini-nesprin2G I128,131A was created by generating the indicated point mutations into GFP-mini-nesprin2G using the Quikchange kit.

The regions containing the CH domains of nesprin2G (aa3-286) were PCR amplified from mRNA isolated from NIH3T3 cells. The PCR product was inserted into pGEX-6P-1 vector (Amersham Biosciences, Piscataway, NJ) after digestion with *Sal*I and *Xba*I to generate GST-CH nesprin2G. Quikchange and the primers used to generate GFP-mini-nesprin2G I128, I131A were re-used to create GST-CH nesprin2G I128, I131A. All primers used to generate DNA constructs used in this paper are described in Table S2. All DNA constructs were confirmed by sequencing.

GST-CH nesprin2 protein and antibody preparation. GST-CH nesprin2G constructs were expressed in E.coli and the tagged proteins purified by standard protocols. For immunization, the GST-CH nesprin2G fragment was further purified by binding to Q-Sepharose 1 ml HiTrap column (Amersham Biosciences) in 50 mM Hepes, pH 8.0 and eluted with a NaCl gradient (0.25-1 M NaCl in 50mM Hepes, pH 8.0). Protein-containing fractions were checked by SDS PAGE and used to immunize rabbits (Pocono Rabbit Farm and Laboratory, Canadensis, PA). Antisera were monitored for reactivity by western blotting and immunofluorescence.

siRNA. All RNAi experiments were performed using 50nM siRNA duplexes (Shanghai GenePharma, Shanghai, China), which were transfected using Lipofectamine RNAiMAX according to the manufacturer (Invitrogen). To identify functional siRNA duplexes, four sequences were selected using the artificial intelligence algorithm, BIOPREDsi (www.biopredsi.org). The duplexes used in this study were the most effective at depleting the target protein based on western blot analysis. The sequences of the duplexes used are described in Table S3.

DNA microinjections. Plasmid DNA was purified using Plasmid Midi Kit (Qiagen, Valencia, CA) and was microinjected into nuclei at a concentration of 10 μg/ml as previously described (*1*).

Epifluorescence live cell microscopy. NIH3T3 fibroblasts were grown on 35 mm dishes with glass coverslip bottoms (homemade or from MatTek Corp., Ashland, MA). Confluent monolayers were starved for 24 h as previously described (*1*). Monolayers were wounded, microinjected with DNA constructs and then incubated (~1-2 h) to allow for expression of the DNA constructs. Cells were then washed twice with live imaging media (HBSS (GIBCO®, Invitrogen) containing essential and nonessential MEM amino acids (Invitrogen), 2.5 g/l glucose, 2 mM glutamine, 1 mM sodium pyruvate, 10 mM HEPES (pH 7.4)), and then stimulated with either LPA or 2% bovine calf serum. Cells were immediately transferred to a Nikon TE300 microscope equipped with a heated (37°C) chamber and a 60× (1.4 NA) plan apo objective (Nikon). Widefield fluorescence and phase-contrast images were collected with TEA/CCD (Princeton Instruments, Trenton, NJ) or Coolsnap HQ (Roper Scientific, Tucson, AZ) cameras controlled by MetaMorph software (Universal Imaging Corporation, Downington, PA). For dual-color fluorescence imaging, cells were transferred to a Nikon TE2000 microscope equipped with perfect focus (Nikon), a heated (37°C) chamber (Oko-lab, Italy), excitation and emission filter wells (Sutter) and a 60x plan apo objective (Nikon). Fluorescence and phase-contrast images were collected with a Coolsnap HQ2 (Roper) camera controlled by MetaMorph software (Universal Imaging. Cells were imaged within 15 min of LPA or serum stimulation.

Cell migration assay. To measure cell migration velocity, starved and wounded monolayers of NIH3T3 fibroblasts in live imaging media were stimulated with 2% CS and then imaged by phase contrast every 30 min over a period of 20 h in multiple fields using a XY stage (Prior, Rockland, MA) on an inverted Nikon TE300 microscope using a 10X phase objective. Average migration velocity was calculated from the average displacement of the wound edge after 20h.

Fluorescence recovery after photobleaching (FRAP). FRAP was performed with a Zeiss LSM 510 META scanning confocal microscope as previously described (*3*).

Immunofluorescence. Coverslips were fixed in either −20°C methanol or paraformaldehyde as previously described (*1, 2*). Secondary antibodies were from Jackson ImmunoResearch Laboratories (West Grove, PA). All images of fixed cells were taken on a widefield epifluorescence microscope.

Determination of nucleus and centrosome position. Fluorescence images of cells stained for pericentrin, β-catenin, DNA, expression tag, and microtubules (Tyr tubulin) were acquired as previously described (*1, 4*). Centrosome orientation to a position between the nucleus and leading edge was determined as previously described (*4*). Analysis of nucleus and centrosome position relative to the cell centroid was performed as previously described (*1*). Briefly, images were pseudocolored, combined and aligned with Metamorph software so that the wound-edge was horizontal. Cell perimeters were drawn over the cell-cell

contacts (stained with β-catenin) and the wound edge (determined from Tyr-tubulin staining and/or injection-markers). From this information, the cell centroid and equivalent radius was calculated using the "integrated morphometry analysis" program in Metamorph. The position of the centrosome was identified by pericentrin staining and marked with the Metamorph "measure pixel" function. The position of center of the nucleus was also marked by estimating the center of the nucleus (observable by negative staining). Next, a vector representing the distances from the nuclear centroid and the centrosome to the cell centroid was drawn and resolved into x and y coordinates (parallel and perpendicular to the leading edge, respectively). Measurements were normalized to cell size by dividing by the average cell radius to allow for comparison between cells. Only the y-coordinate was used in plots as the x-coordinate (position of the nuclear centroid or centrosome along the x-axis) did not change significantly.

Actin pelleting assay. Aliquots of 10 μM G-actin were polymerized at room temperature for 45 min in G-buffer (10mM Tris-HCl pH 7.5, 0.2mM $CaCl_2$, and 0.2mM DTT) containing 2mM $MgCl_2$, 50mM KCl, 0.5mM ATP, and 0.3μM phalloidin. The resulting polymerized F-actin was resuspended with or without 10 μM GST-nesprin2G CH domain in 10mM Tris-HCl pH 7.5, and 50mM NaCl and incubated at room temperature for 15 min. F-actin was sedimented at 90,000 rpm in a TLA120 rotor (Beckman Coulter) for 20 min at 20°C. Resulting supernatants and pellets were resuspended in sample buffer and analyzed by western blotting for either actin or GST. Before use, all proteins were precleared at 90,000 rpm in a TLA120 for 20 min at 4°C.

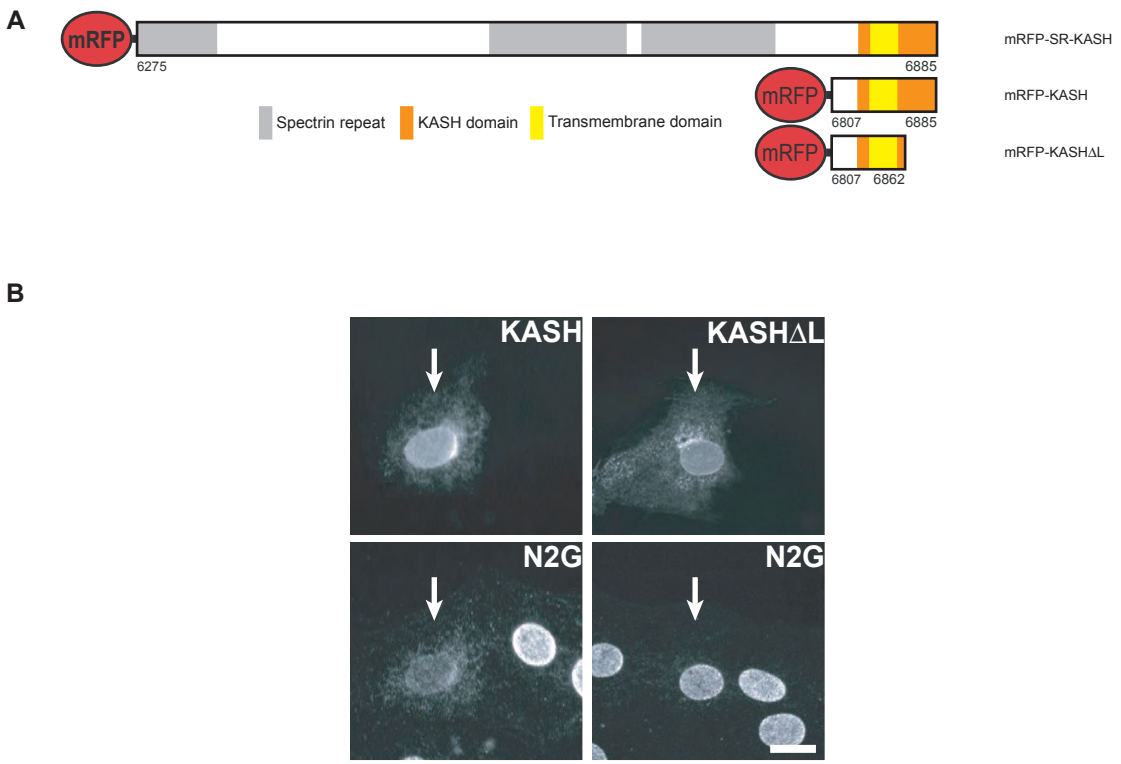

Fig. S1: mRFP-KASH domain constructs disrupt nuclear localization of endogenous nesprin2G. **A**, Diagram of dominant negative (SR-KASH and KASH) and control KASH (KASHΔL) constructs derived from human nesprin2. Protein domains and positions were derived using the SMART platform (*5*). Amino acids positions are based upon the human nesprin2G isoform (6885 aa). **B**, LPA-stimulated, wound-edge NIH3T3 fibroblasts expressing the indicated constructs after DNA microinjection into the nucleus. Fixed cells were stained for endogenous nesprin2G (N2G) and expression of the KASH construct was confirmed by mRFP fluorescence. White arrows indicate expressing cells. Bar, 10μm.

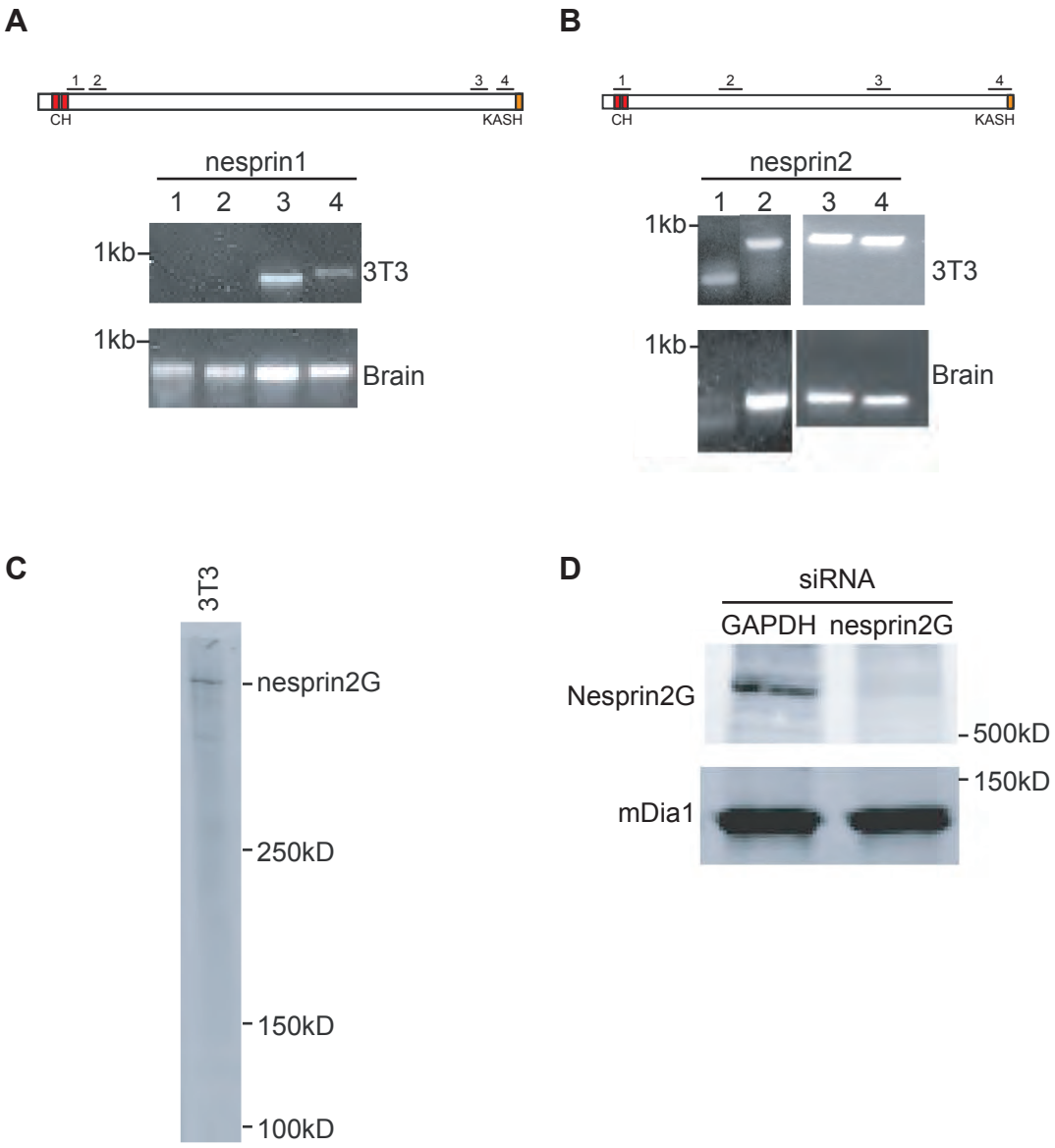

Fig. S2: Identification of nesprin isoforms in NIH3T3 fibroblasts. **A**,**B**, Diagrams of mouse nesprin1G and nesprin2G full length cDNAs are shown above the DNA gels. Numbered black lines above the diagrams represent the region amplified by individual RT-PCR primer pairs. The results of RT-PCR using the indicated primer pairs and mRNA from NIH3T3 fibroblast or mouse brain are located below the diagrams. Note that products corresponding to regions in nesprin 2G, but not nesprin 1G, were identified in NIH3T3 fibroblasts. **C**, Western blot of a NIH3T3 fibroblast lysate using the anti-nesprin-2G CH domain antibody. **D**, Western blot of NIH3T3 fibroblasts depleted of either GAPDH or nesprin2G probed with anti-nesprin2G CH domain. Western blot with mDia1 is shown as a loading control.

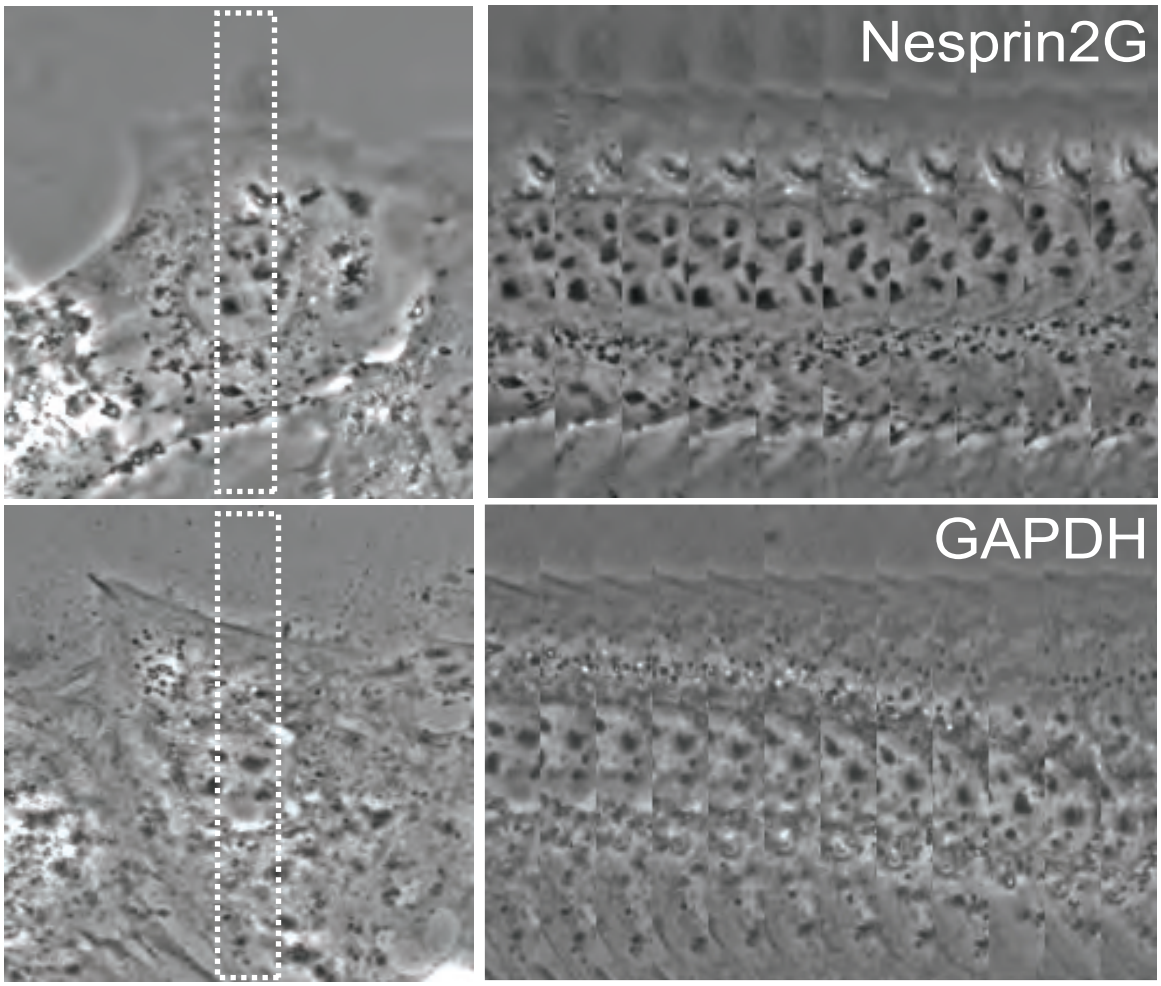

Fig. S3: Nesprin2G is required for nuclear movement. Sequential phase contrast images from movies of LPA-stimulated wound-edge, NIH3T3 fibroblasts depleted of either GAPDH or nesprin2G. Images to the left show the starting frames from which the kymographs (5 min/frame) to the right were constructed. The dashed boxes indicate the region used to generate the kymographs. Movies were begun 15 min after LPA stimulation. Note that the nucleus moves away from the leading edge and toward the back of the cell in the GAPDH depleted control, but does not move in the nesprin2G depleted cell. Bar, 5 μm.

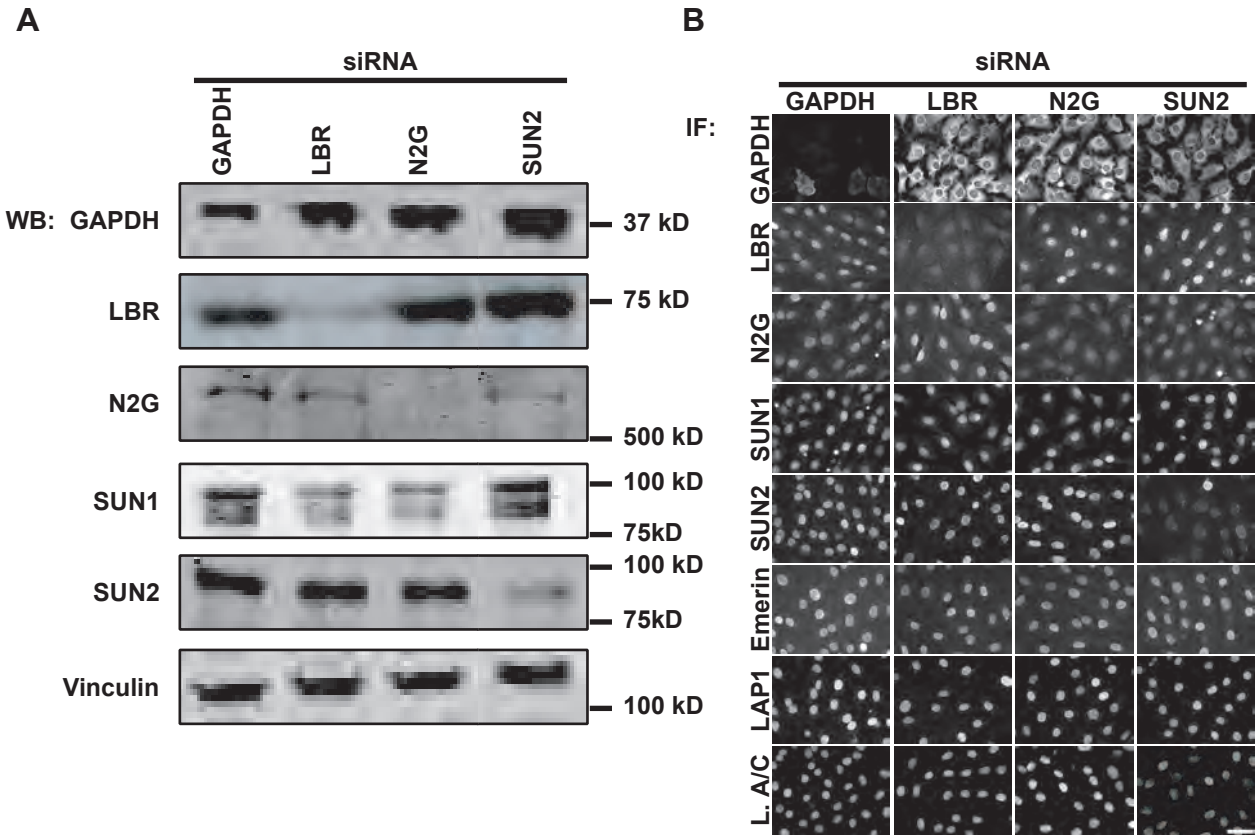

Fig. S4: Evaluation of siRNA-mediated knockdown of LINC complex components. **A**, Western blots (WB) of lysates from NIH3T3 fibroblasts transfected with the indicated siRNAs and grown for 3 d following transfection. Vinculin was used as a loading control (each WB was controlled for loading with vinculin, but only one is shown here). **B**, Immunofluorescence (IF) images of NIH3T3 fibroblasts depleted of the indicated proteins using siRNA. Cells were stained with antibodies against GAPDH, lamin B receptor (LBR), nesprin2G (N2G), SUN1, SUN2, emerin, LAP1, and lamin A/C (L. A/C). Bar, 20 μm.

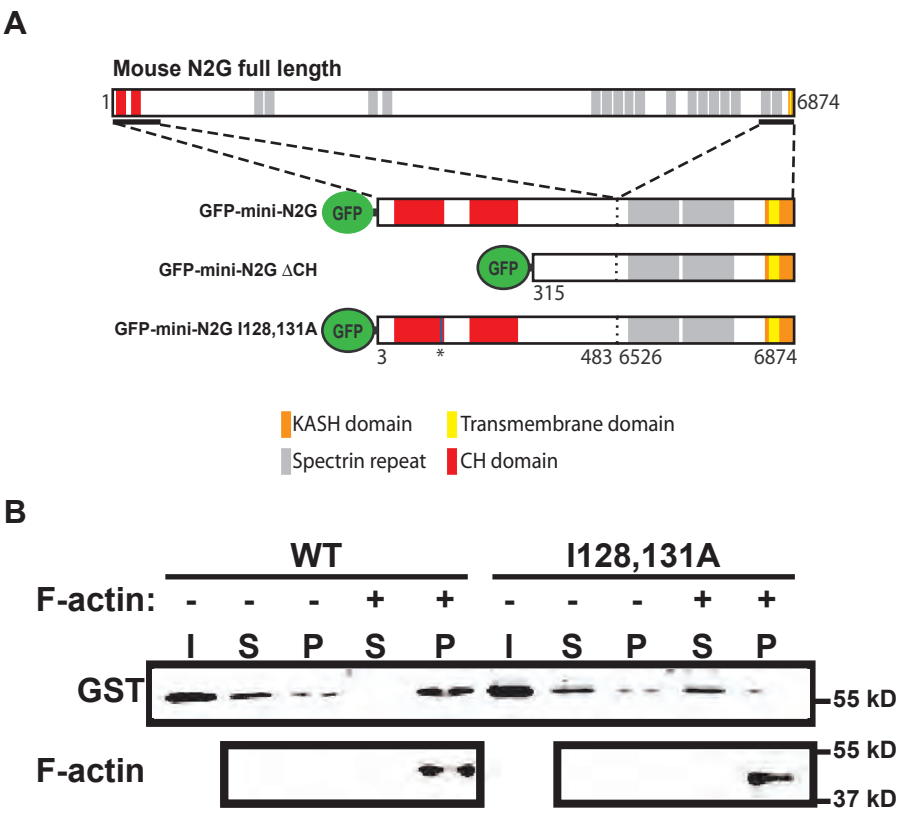

Fig. S5: Characterization of GFP-mini-nesprin2G constructs. **A**, Diagram of full length mouse nesprin2G (N2G) and GFP-mini-N2G constructs used in this paper. Protein domains and positions were derived using the SMART platform (*5*). GFP-mini-N2G is an N-terminally GFP-tagged construct consisting of the N-terminal CH domains of nesprin2G fused to a C-terminal domain containing the last two spectrin repeats and the KASH domain of nesprin2G. Three silent nucleotide substitutions were incorporated to render the construct insensitive to siRNA. GFP-mini-N2G ΔCH lacks the N-terminal CH domains as indicated. GFP-mini-N2G I128,131A contains two point mutations (blue line and asterisk) within the first CH domain. Numbers indicate amino acid residues of segment boundaries based upon full length mouse nesprin2G. **B**, The CH domain of nesprin2G binds actin and requires I128 and I131. Western blot of co-sedimentation of GST-WT or GST-mutant (I128,131A) nesprin2G CH domains with polymerized F-actin. GST-CH domain constructs were incubated with or without polymerized actin (F-actin) and then pelleted by ultracentrifugation. Equivalent amounts of the input (I), supernatant (S), and pellets (P) were loaded and western blots were probed for GST or actin.

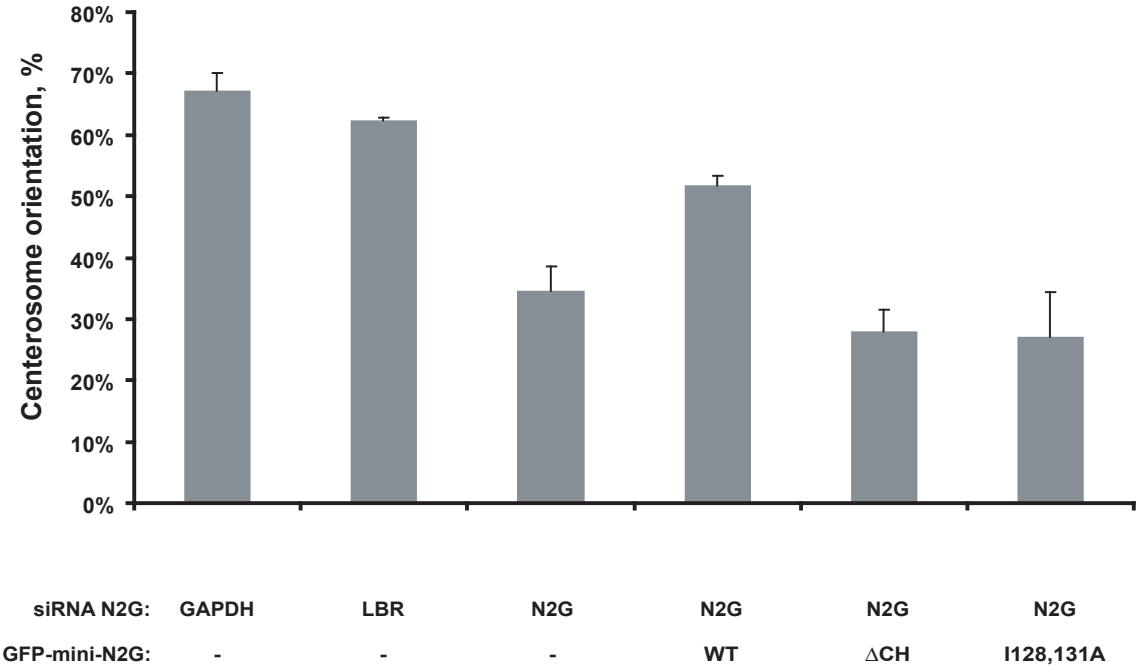

Fig. S6: Nesprin2G is required for centrosome orientation and GFP-mini-N2G expression rescues nesprin2G-depletion. Quantification of centrosome orientation in LPA-stimulated, wound-edge siRNA-treated NIH3T3 fibroblasts depleted of GAPDH, lamin B receptor (LBR), or nesprin2G (N2G) following LPA-stimulation. Expressed GFP-mini-N2G in nesprin2G depleted cells is indicated. Centrosome orientation was determined as previously described (*4*). Experiments were repeated ≥ 3 times with N>30. Error bars are SEM.

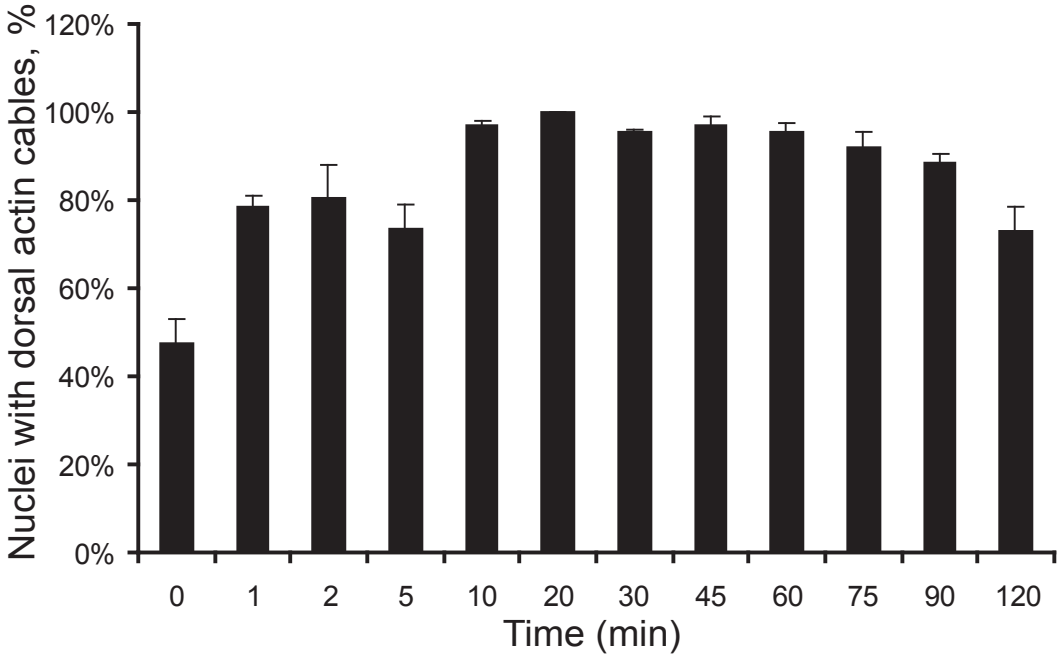

Fig. S7: Presence of dorsal actin cables on nuclei following LPA stimulation. Quantification of the average percentage of nuclei in wound edge cells associated with one or more dorsal actin cables following LPA stimulation for the indicated times. A nucleus was scored positive if the dorsal actin cables spanned the nucleus. Experiments were repeated 3 times with N > 151. Error bars are SEM.

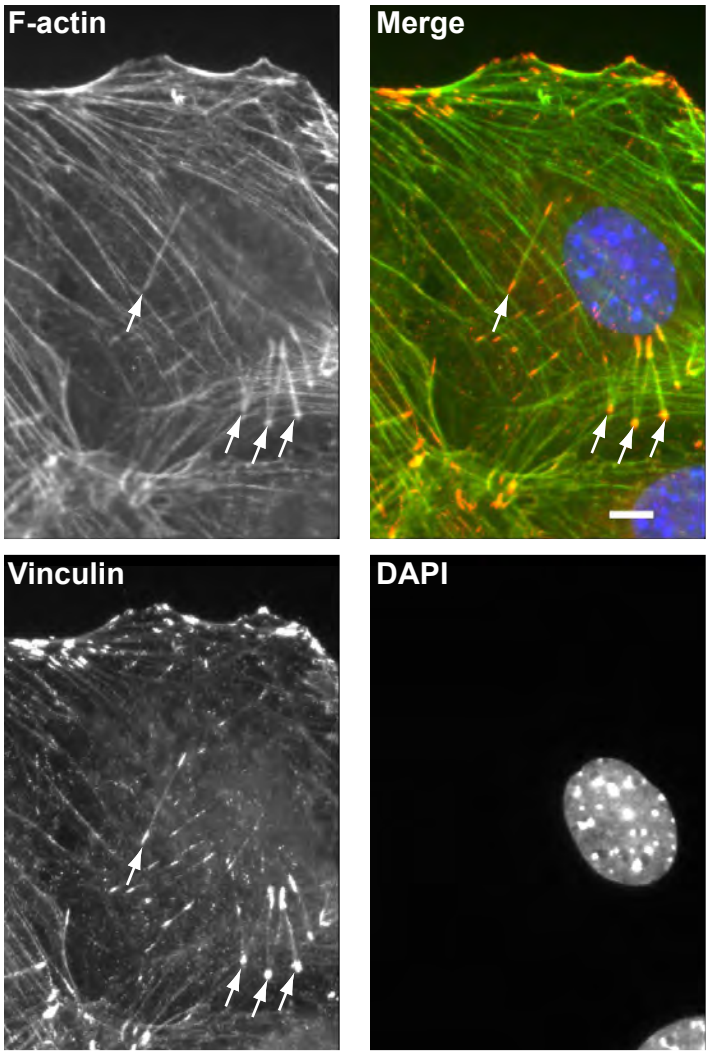

Fig. S8: Ventral actin cables terminate in focal adhesions. Representative fluorescent images of wound edge NIH3T3 fibroblasts after one hour of LPA stimulation. Actin was stained with rhodamine-phalloidin (F-actin), nuclei/DNA with DAPI, and focal adhesions with vinculin. Arrows indicate ventral actin cables associated with vinculin. These images were taken at lower magnification to reveal both dorsal and ventral actin cables. Bar: 10 μm.

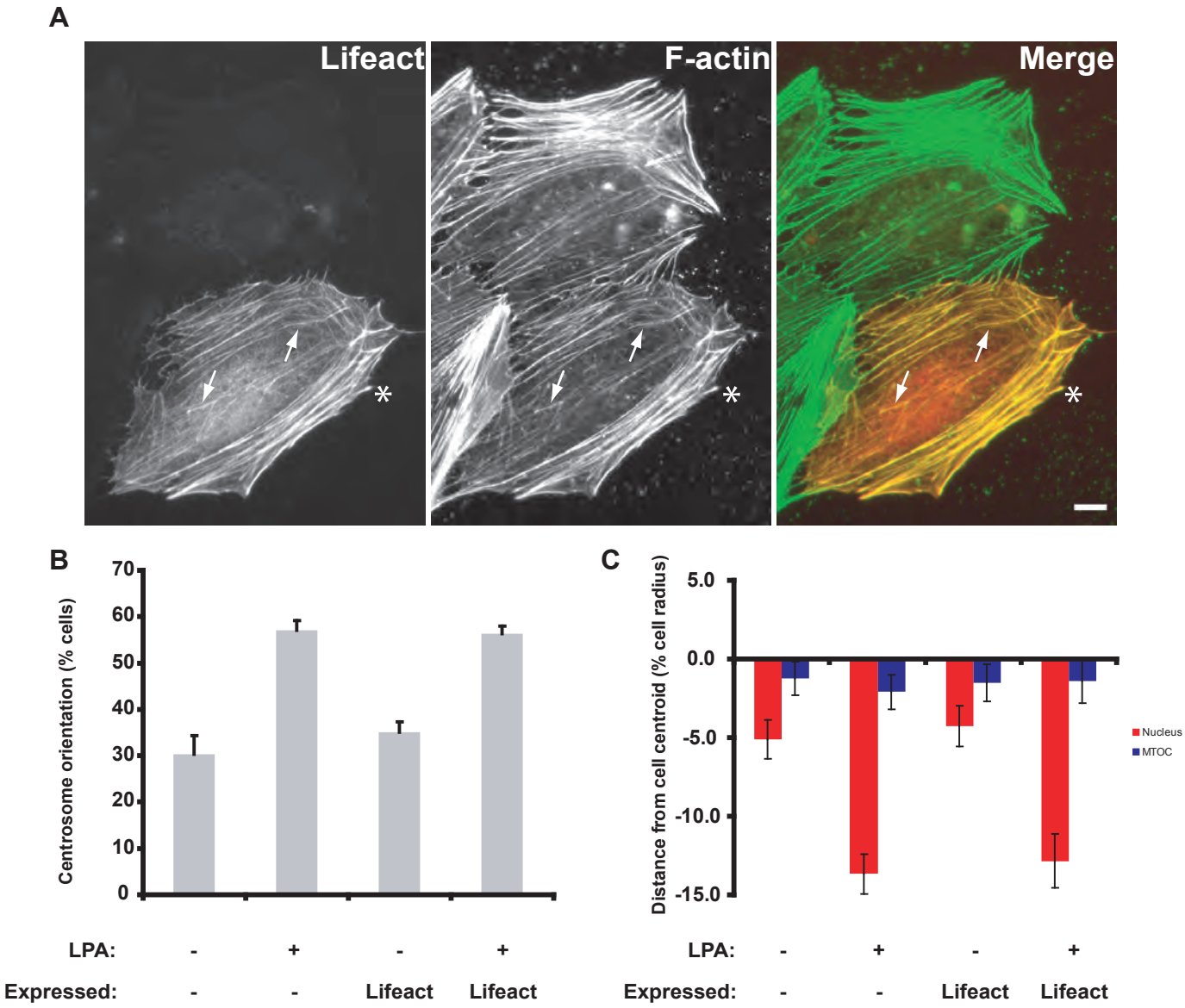

Fig. S9: Use of Lifeact-mCherry as a probe for actin dynamics in NIH3T3 fibroblasts. **A**, Representative fluorescent images of a fixed NIH3T3 fibroblast expressing Lifeact-mCherry (asterisk) and stained for actin with FITC-phalloidin. Lifeact-mCherry does not significantly alter the organization of actin filaments (compare expressing cell with neighboring cells) and labels the same filaments as phalloidin. Arrows indicate actin filaments labeled by Lifeact-mCherry and phalloidin. **B**, Comparison of centrosome orientation in wound-edge NIH3T3 fibroblasts expressing or not expressing Lifeact-mCherry. Cells were stimulated with LPA as indicated. Experiments were repeated at least 3 times with N>179. Error bars are SEM. **C**, Comparison of average centrosome and nucleus positions from cells described in **B**.

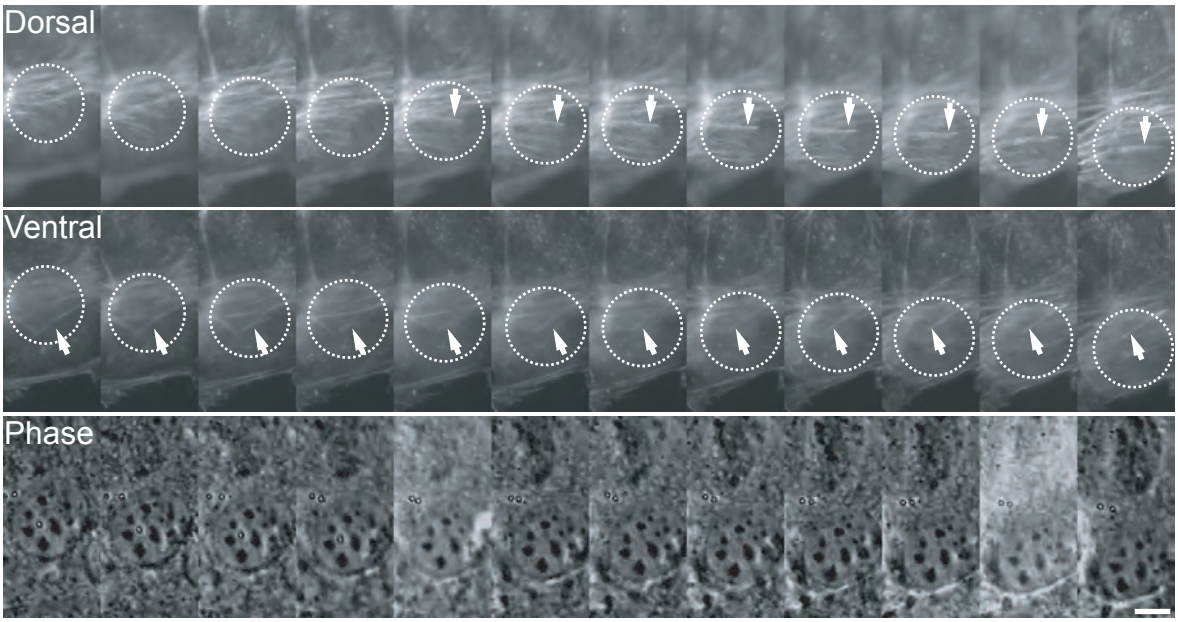

Fig. S10: Complete phase and fluorescent kymographs of the LPA-stimulated wound edge NIH3T3 fibroblasts expressing Lifeact-mCherry described in **Fig. 2C**. Fluorescent images were acquired from dorsal and ventral planes of the fibroblast as indicated. An outline of the nucleus (from the corresponding phase image) is given by the dashed white line. The leading edge of the cell is oriented toward the top of the panels. Panels are every 5 min. Time: hr:min. Bar: 5 μm. Wound edge is towards the top of the images.

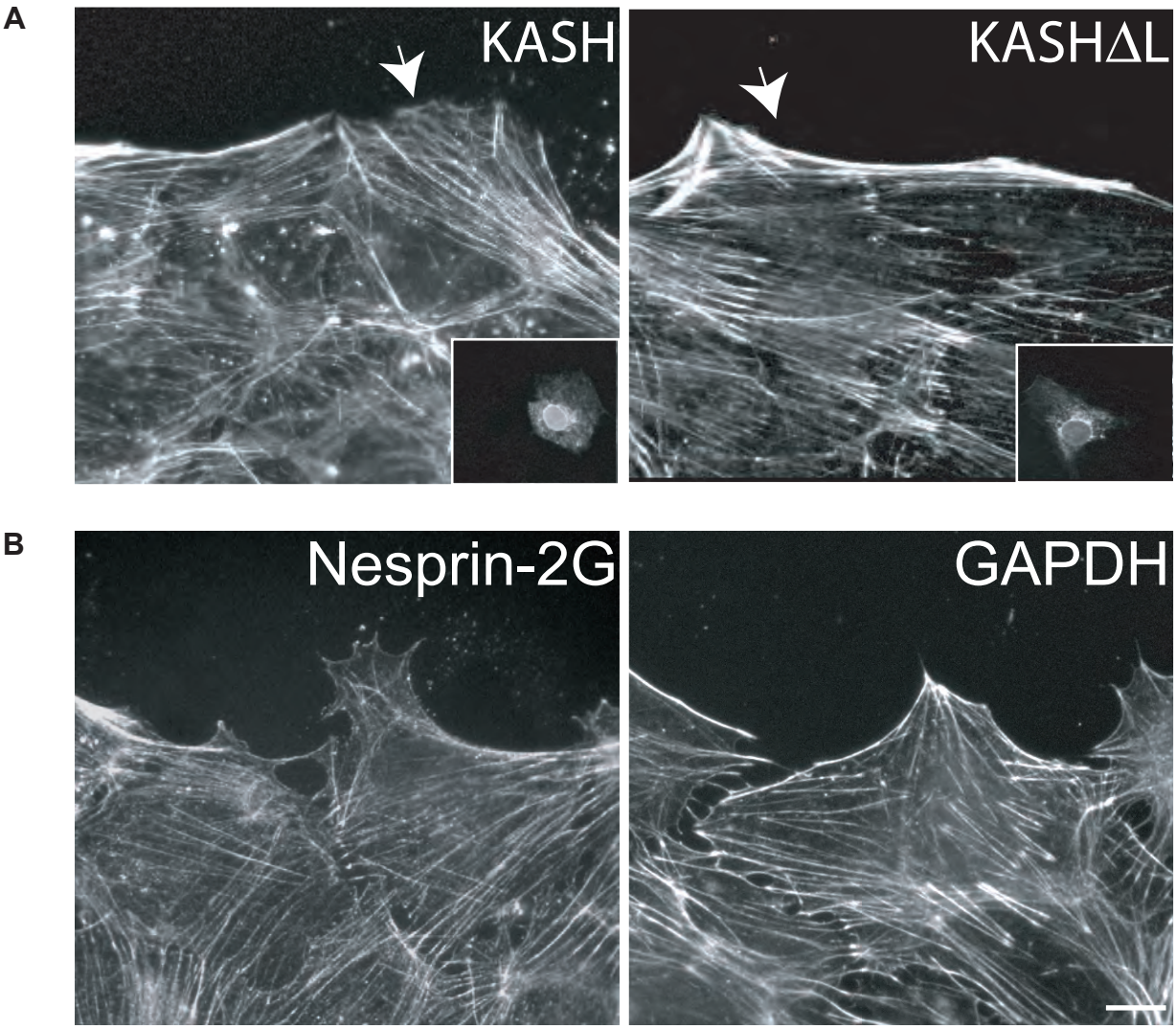

Fig. S11: The organization of the actin cytoskeleton is not grossly perturbed by KASH domain expression or nesprin2G-depletion. **A**, Fluorescence images of LPA-stimulated, wound edge NIH3T3 fibroblasts expressing either the RFP-KASH or RFP-KASHΔL constructs and stained with Alexa488-phalloidin to reveal actin filaments. Insets show RFP fluorescence indicating cells expressing KASH constructs. Arrows indicate expressing cells. **B**, Fluorescence images of LPA-stimulated, wound-edge NIH3T3 fibroblasts depleted of either GAPDH or nesprin2G. Cells were stained with Alexa488-phalloidin. Bar: 10 μm.

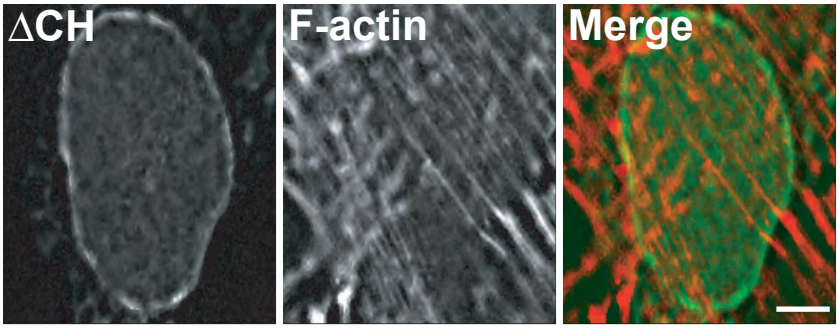

Fig. S12: The CH domains of GFP-mini-nesprin2G are required for TAN line formation. Fluorescence images of the dorsal nuclear surface of a wound-edge NIH3T3 fibroblast depleted of nesprin2G and expressing GFP-mini-N2G ΔCH. The cell was stimulated with LPA and fixed and stained for GFP (ΔCH) and filamentous actin with rhodamine phalloidin (F-actin). The cell leading edge is toward the upper right. Bar: 5 μm.

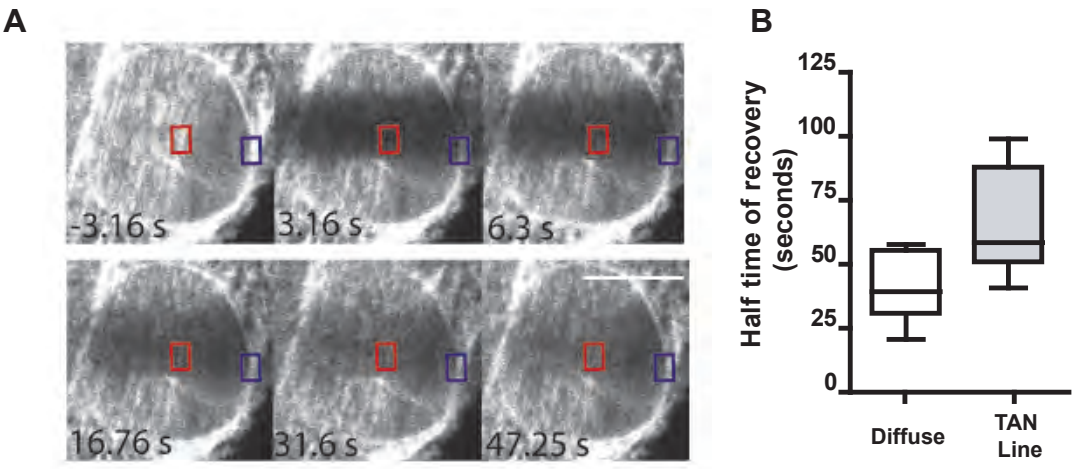

Fig. S13: GFP-mini-N2G is less mobile in TAN lines that in the bulk nuclear membrane. **A**, Confocal fluorescence images from a representative FRAP experiment of GFP-mini-nesprin2G on the dorsal surface of LPA-stimulated, wound-edge NIH3T3 fibroblasts depleted of nesprin2G. The red and blue boxes show regions monitored to determine the half time of fluorescence recovery in TAN lines and bulk membrane, respectively. Time pre- and post-FRAP is in sec. **B**, Average half-time of recovery of GFP-mini-N2G fluorescence in TAN lines and in diffuse, nuclear envelope following photobleaching. Data are from 3 independent experiments (N=36 cells per experiment; error bars are SEM). Bar: 5 μm.

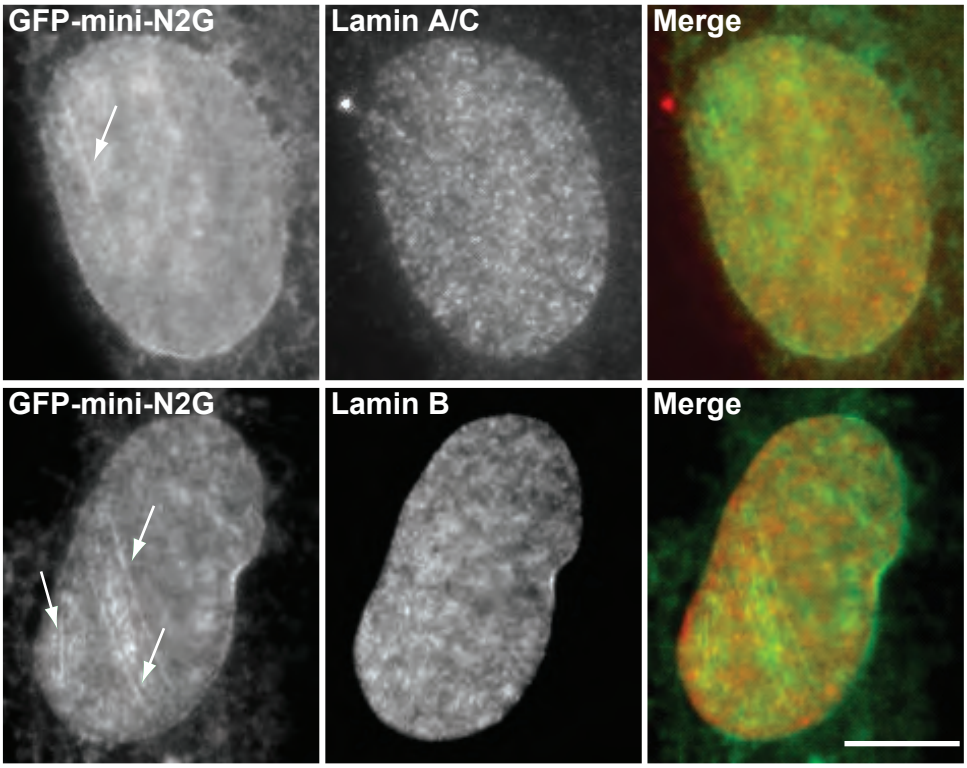

Fig. S14: Nuclear lamins are not recruited to TAN lines. Fluorescence images of fixed cells showing the lack of recruitment of endogenous lamin proteins (lamin A/C or lamin B) to GFP-mini-N2G TAN lines on the dorsal surface of nuclei in nesprin2G-depleted NIH3T3 fibroblasts. Lamins and GFP were stained with specific antibodies. Arrows indicate GFP-mini-N2G TAN lines. The cell leading edge is toward the upper right. Bar: 5 μm.

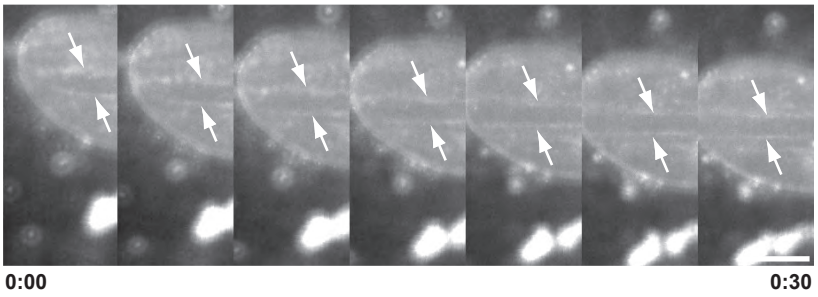

Fig. S15: GFP-SUN2 forms TAN lines and moves rearward with the nucleus. Fluorescence kymograph of GFP-SUN2 TAN lines in a LPA-stimulated wound edge NIH3T3 fibroblast. Arrows indicate individual TAN lines. Each frame is 5 min. Time: hr:min. The leading edge is oriented towards the top of each image. Bar: 5 μm.

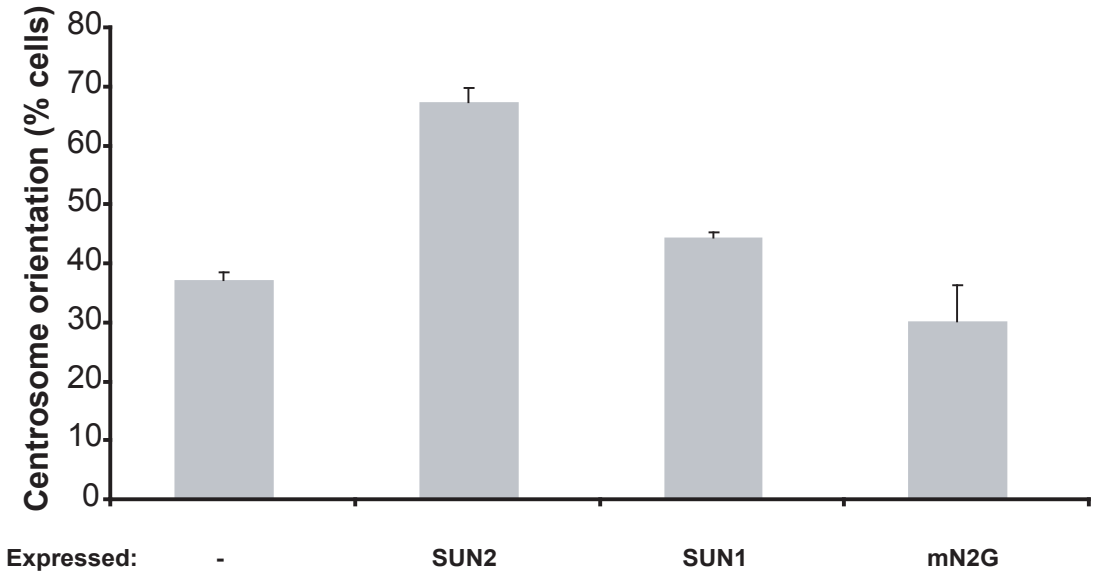

Fig. S16: Centrosome orientation is rescued in SUN2 depleted cells by expressing GFP-SUN2, but not GFP-SUN1 or GFP-mini-N2G. Quantification of centrosome orientation in LPA-stimulated, wound-edge NIH3T3 fibroblasts depleted of SUN2 using siRNA and expressing the indicated constructs. Experiments were repeated at least 3 times with N>66. Error bars are SEM.

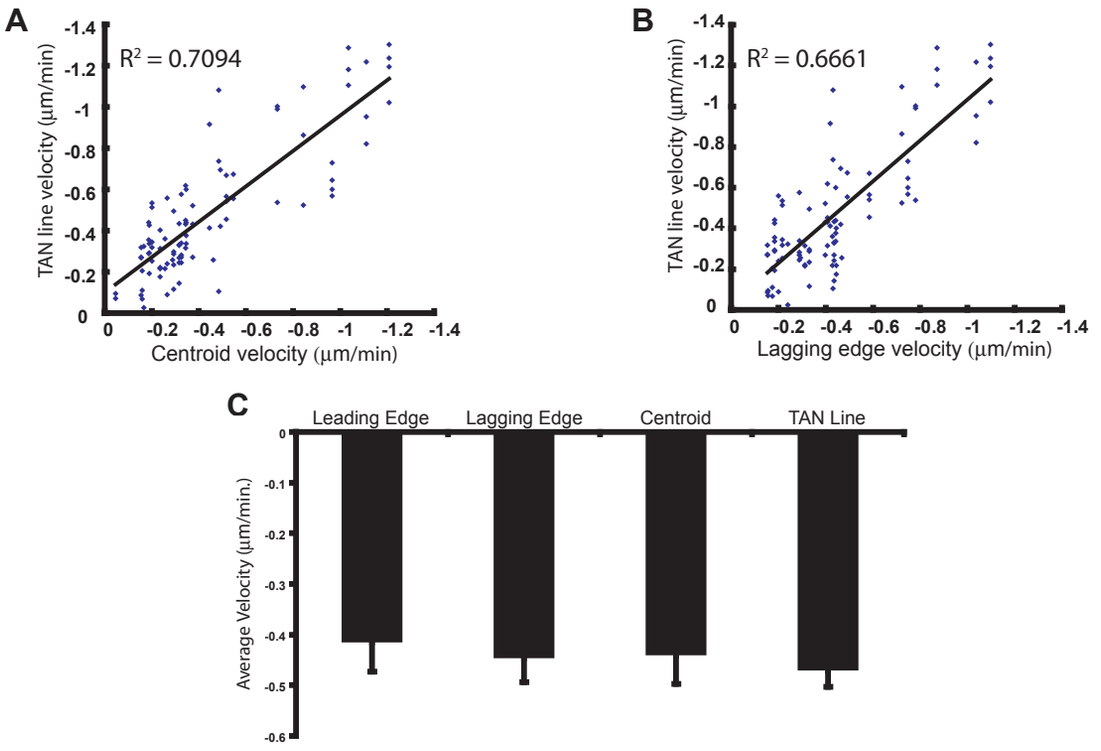

Fig. S17: Analysis of TAN line and nuclear movement reveals coordinated movement. **A**,**B,** Velocity of GFP-mini-nesprin2G TAN lines compared to that of the lagging edge and centroid of the nucleus in LPA-stimulated, wound-edge NIH3T3 fibroblasts depleted of nesprin2G. R2 is the coefficient of determination. **C**, Average velocities of GFP-mini-nesprin2G TAN lines compared to the leading edge, lagging edge, and centroid of the nucleus. Data are from 30 movies of 30 cells. Error bars are SEM.

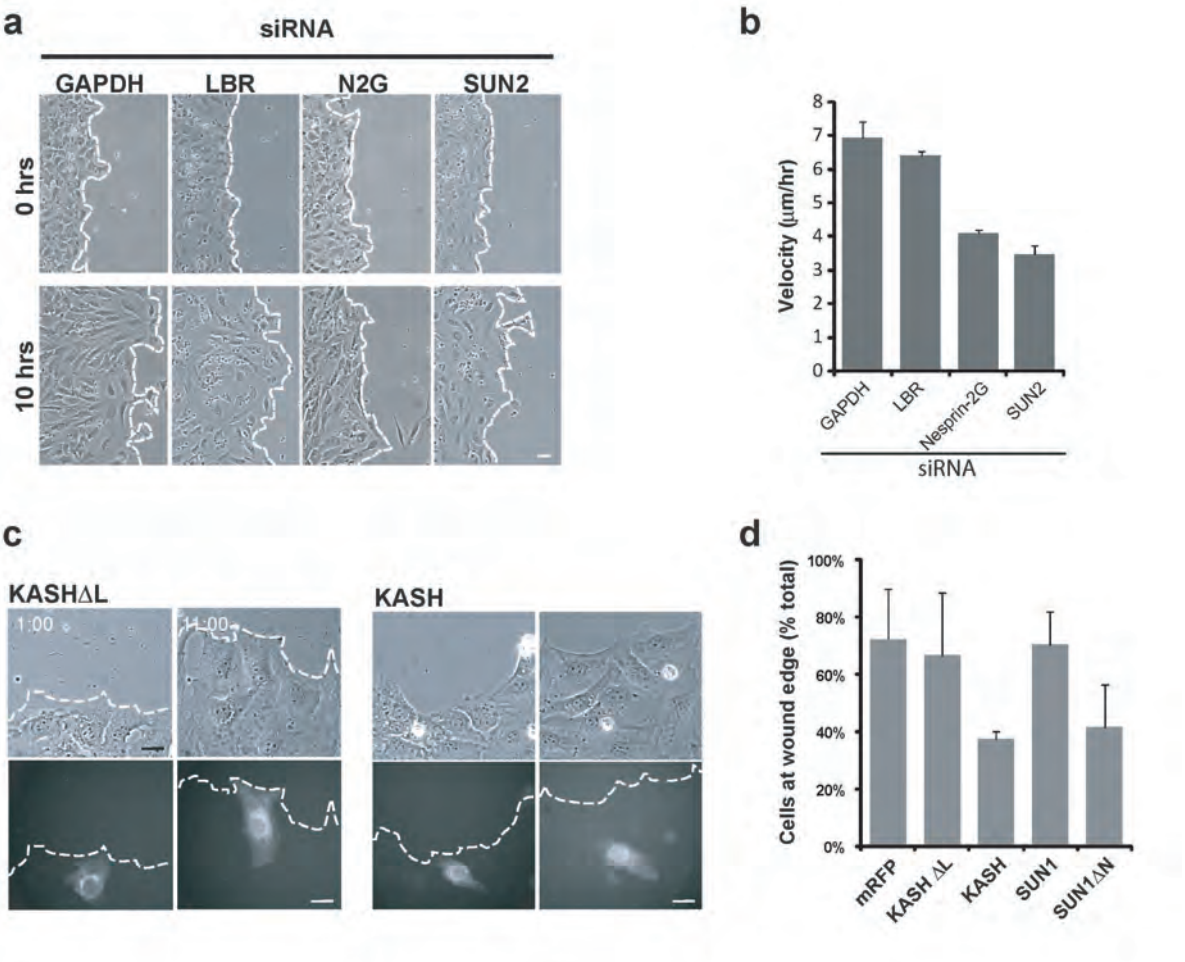

Fig. S18: Directed migration of NIH3T3 fibroblasts into a wound requires LINC complex components. **A**, Representative phase contrast images of serum-stimulated, wound-edge NIH3T3 fibroblasts depleted of the indicated proteins. Panels show the cells just before (0 h) serum-stimulation and 10 h later. The edge of the wound is indicated by dashed, white lines. **B**, Quantification of the average velocity (μm/hr) of migration for the cells described in **A**. Data is from three independent experiments with at least five wound-edges measured per condition. **C**, Representative phase and fluorescence images of serum-stimulated, wound-edge NIH3T3 fibroblasts expressing control RFP-KASHΔL or dominant negative RFP-KASH at 1 hr and 11 h after expression. The edge of the wound is indicated by dashed, white lines. Note that the RFP-KASHΔL expressing cell stays at the wound-edge, whereas the RFP-KASH expressing cell falls behind. **D**, Percentage of cells in **C** expressing the indicated constructs present at the wound-edge 20 h after stimulation with 2% serum. Data is from two independent experiments with N>20. Error bars in **B** and **D** are SEM. Bars, **A**: 20 μm and **C**: 10 μm.

Gene	Location	Forward primer	Reverse primer
nesprin1	1	TGCAAAGAGATGGCAAACTG	GTTGGAGATCACCTCCTCCA
nesprin1	2	TTCATGAGTGAAGCCACTGC	AACAGTGGGGAGCAACATTC
nesprin1	3	AAGACTCCACGGCTCTTTCA	GCCACTTCTGAAGGTTCTGC
nesprin1	4	GAACCTTCAGAAGTGGCAG	GGTTTCCAATCACATGGACC
nesprin2	1	ATGCGCTTGGTTCATGTATC	TGACCCCTTACAGGCCTTGT
nesprin2	2	ATCAGAACCTGCGGGATATC	ACTTTTTCCGATGCTTCACG
nesprin2	3	GGAAGCTCACGAAATCCAAA	AGAATCTTCCAGAGCCATCTG
nesprin2	4	TGATGGTCTCCGTCAATGTG	GGCGCATTAGGTCTTTCTGA

Table 1: RT-PCR primers for detecting expression of LINC complex members. Location referes to the position where the primer interacts with its cognate gene as depicted in **Fig. S2**.

Primer name	Sequence	Enzyme	Vector
SR-KASH-F	TCAGAGAGTGACGCC	*Sal*I	pmRFP-C1
SR-KASH-R	CTATGTGGGGGGTGGC	*Bam*HI	pmRFP-C1
KASH-F	ACTACAGAAGGCGAGGAGGAGACA	*Sal*I	pmRFP-C1
KASH-R	CTATGTGGGGGGTGGC	*Bam*HI	pmRFP-C1
KASHΔL-F	ACTACAGAAGGCGAGGAGGAGACA	*Sal*I	pmRFP-C1
KASHΔL-R	CTAGCAGCTGTAGTCTTCTTCGGAGGA	*Bam*HI	pmRFP-C1
Nt-mini-nesprin2G-F	GCTAGCCCTGTGCTGCCCA	*Sal*I	-
Nt-mini-nesprin2G-R	CTACTCCAGGAGTGGGATGAAG	*Xba*I	-
Ct-mini-nesprin2G-F	GACAGGTGGGAGCTGATCCA	*Sal*I	-
Ct-mini-nesprin2G-R	CTAGGTGGGAGGTGGCCCGTT	*Xba*I	-
mini-nesprin2G SOEing Overlap-F	CTTCATCCCACTCCTGGAGCTTCACAGCAAGC	-	-
mini-nesprin2G SOEing Overlap-R	GCTTGCTGTGAAGCTCCAGGAGTGGGATGAAG	-	-
mini-nesprin2G SOEing-F	GCTAGCCCTGTGCTGCCCA	*Sal*I	pEGFP-C1
mini-nesprin2G SOEing-R	CTAGGTGGGAGGTGGCCCGTT	*Xba*I	pEGFP-C1
siRNA resistant mini-nesprin2G-F	GGCCTGATCTGGAC**G**AT**T**AT**T**CTGCACTTTCAT ATTGAGAAGCTC	-	-
siRNA resistant mini-nesprin2G-R	GAGCTTCTCAATATGAAAGTGCAGAATAATCG TCCAGATCAGGCC	-	-
mini-nesprin2GΔCH-F	GATTCCACACAGGCCAAGG	*Sal*I	pEGFP-C1
mini-nesprin2GΔCH-R	CTAGGTGGGAGGTGGCCCGTT	*Xba*I	pEGFP-C1
mini-nesprin2G I128,I131A-F	CCATTATCCTTGGCCTG**GCT**TGGACC**GCT**ATC CTGCACTTTCATATTG	-	-
mini-nesprin2G I128,I131A-R	CAATATGAAAGTGCAGGATAGCGGTCCAAGCC AGGCCAAGGATAATGG	-	-
nesprin-2G CH-F	GAGCAGGAGGACACTCAGAAGA	*Bam*HI	pGEX-6P-1 pMAL-c2X
nesprin-2G CH-R	CTACGAATACTTCAGGAACTGCG	*Sal*I	pGEX-6P-1 pMAL-c2X
SUN2-F	ATGTCGAGACGAAGCCAGC	*Sal*I	pEGFP-C1
SUN2-R	GTGGGCAGGCTCTC	*Xba*I	pEGFP-C1

Table 2: Primers used to generate the constructs used in this paper. The F or R in the primer name refers to forward or reverse, respectively. When applicable, primers have a 5' GC-clamp followed by a restriction enzyme recognition sequence preceding the given

Gene	siRNA sequence
GAPDH	AAAGUUGUCAUGGAUGACCTT
LBR	GAGUAACAGCACUAUUUAATT
nesprin2G	CCAUCAUCCUGCACUUUCATT
SUN2	GGGUCAUUCUGCAGCCAGATT

Table S3: Sequences of siRNA duplexes used in this paper. The reverse sequence is not shown.

Supplementary Material References:

1. E. R. Gomes, S. Jani, G. G. Gundersen, *Cell* **121**, 451 (May 6, 2005).
2. A. F. Palazzo, T. A. Cook, A. S. Alberts, G. G. Gundersen, *Nat Cell Biol* **3**, 723 (Aug, 2001).
3. A. S. Infante, M. S. Stein, Y. Zhai, G. G. Borisy, G. G. Gundersen, *J Cell Sci* **113 (Pt 22)**, 3907 (Nov, 2000).
4. A. F. Palazzo *et al.*, *Curr Biol* **11**, 1536 (Oct 2, 2001).
5. J. Schultz, F. Milpetz, P. Bork, C. P. Ponting, *Proc Natl Acad Sci U S A* **95**, 5857 (May 26, 1998).